Iranian Journal of Catalysis 8(1), 2018, xx-xx

IRANIAN JOURNAL OF CATALYSIS

Visible light induced photocatalytic degradation of direct red 23 and direct brown 166 by $InVO_4$-TiO_2 nanocomposite

Somayeh Dianat*

Department of Chemistry, Faculty of Sciences, University of Hormozgan, Bandar Abbas 71961, Iran.

Received 24 October 2017; received in revised form 6 January 2018; accepted 29 January 2018

ABSTRACT

The effect of various parameters (pH, irradiation time, nanophotocatalyst dosages and temperature) on photocatalytic degradation of Direct Red 23 (DR 23) and Direct Brown 166 (DB 166) using pure $InVO_4$ and $InVO_4$-TiO_2 nanocomposite were investigated under visible light irradiation. $InVO_4$ and $InVO_4$-TiO_2 were synthesized by hydrothermal and sol-gel/ hydrothermal treatment techniques, respectively and characterized by FT-IR spectroscopy, x-ray diffraction (XRD), diffuse reflectance UV–vis spectroscopy (DRS), scanning electron microscopy (SEM) and transmission electron microscopy (TEM) images. Doping of TiO_2 with $InVO_4$ caused reduction in its band gap value with the resultant improvement in its visible light activity. The efficiency of nanocomposite on azo dyes degradation (pH 7.2, time: 30 min) reached high values (above 95%) under visible light, proving the remarkable photocatalytic activities of obtained composites. Moreover, the results indicated complete mineralization of DR 23 and DB 166 by $InVO_4$- TiO_2 under visible light for 300 min.

***Keywords**: Degradation, Mineralization, Azo dye, $InVO_4$, $InVO_4$-TiO_2.*

1. Introduction

Organic dyes used in textile and food industries are important sources of the environmental contaminations due to their non-biodegradability and high toxicity to aquatic creatures and carcinogenic effects on humans [1-5]. Hence, it is critical to remove these dyes from colored effluents [6]. To this end, a variety of biological and physicochemical methods for wastewater treatment has been developed (e.g., adsorption on activated carbon, ultrafiltration, reverse osmosis, coagulation by chemical agents, ion exchange on synthetic adsorbent resins, etc.) [7-9]. Among the various wastewater treatment technologies, advanced oxidation processes (AOPs) have received much attention in recent years. AOPs in which the high oxidizing potential of species such as hydroxyl radicals is utilized, have been proposed as an alternative way for the complete elimination and full mineralization of undesirable organic pollutants including dyestuffs [10,11].

*Corresponding author emails: s.dianat@hormozgan.ac.ir s_dianat60@yahoo.com
Tel.: +98 76 3766 0063; Fax: +98 76 3667 0714

Semiconductor-mediated photocatalysis is one of the most efficient destructive technologies among AOPs for the degradation of various families of organic pollutants [12,13]. Among the photocatalysts, TiO_2 has been intensively investigated as a semiconductor photocatalyst because of its stability, cheapness and environmental friendliness. Unfortunately, a major impediment in the popularization of this semiconductor material is the large band gap, 3.2 eV for bulk TiO_2. This severe disadvantage limits the photocatalyst photosensitivity to the ultraviolet region, a small fraction (~5%) of the solar energy. Therefore, significant efforts have been made to develop stable and efficient photocatalysts which are capable of using abundant visible light in solar spectrum or artificial light sources [14-20]. Furthermore, TiO_2 presents a relatively high electron-hole recombination rate which is unfavorable to its photoactivity [21]. Therefore, suppression of the recombination of photo-generated electron-hole pairs in TiO_2 is essential for improving the efficiency of photocatalytic activity. For this purpose, doping TiO_2 with various noble/transition metal or metal ions and their photocatalytic activities has been

investigated extensively [22-25]. Some theoretical calculations have also been performed to suggest that doping of TiO_2 has a considerable effect on the band gap alteration and photocatalytic activity [14]. In doped-TiO_2 systems, excited by UV or visible light with sufficient energy, sensitizer adsorbed on TiO_2 injects electron into the conduction band (CB) of TiO_2, which acts as a mediator for transferring electrons from the excited sensitizer to the electron acceptors on TiO_2 surface, while the holes are injected in opposite direction between valence bands. Doped semiconductor systems have a high ability to shift the required energy for excitation of coupled system towards longer wavelengths [21,26,27]. Traditional sensitizers are small band-gap semiconductors or organic dyes. Some of these systems have achieved high quantum efficiencies [28,29]. The key challenge in sensitization-type photocatalysis is finding sufficiently stable sensitizers with appropriate electronic states. Stable multimetallic oxides (e.g. $InMO_4$ [M =V, Nb, or Ta]) have recently attracted much attention as new photocatalytic materials for hydrogen generation from water splitting under visible light irradiation [19, 30-32].

In our previous work, photocatalytic activity of $InVO_4$ and $InVO_4$–TiO_2 nanoparticles in the degradation of aqueous solutions of industrial textile azo dyes and also formaldehyde (FAD) under visible light and ultrasonic irradiations has been compared [33]. In the continuing and for purpose of extension of our research in this area, the visible light photoactiviy of $InVO_4$-TiO_2 nanocomposite for the photodegradation of two other types of non-biodegradable azo dyes such as Direct red 23 (DR 23) and Direct Brown 166 (DB 166) was investigated in this work. Moreover, a comparative study in electrical properties of $InVO_4$ and $InVO_4$–TiO_2 is evaluated by diffuse reflectance UV–Vis spectroscopy (DRS) and potentiometric mass titrations methods for estimation of band gap energy and point of zero charge (pzc), respectively.

2. **Experimental**

2.1. Reagents and materials

The $InVO_4$ nanocatalyst and $InVO_4$-TiO_2 nanocomposite were prepared according to the literature [33]. Sodium metavanadate, indium (III) chloride, titanium tetraisopropoxide, isopropyl alcohol, DR 23 and DB 166 and other chemicals were of analytical grade purchased from commercial sources (Merck or Sigma) and used without further purification. Their chemical structures and other characteristics are listed in Table 1. All of the reagents and solvents were analytical grade and used without further purification. The pH value of solutions was adjusted with 0.05 mol L^{-1} HCl and 0.2 mol L^{-1} NaOH solutions and doubly distilled water was used for dye solution preparation.

2.2. Physical measurements

Elemental analysis of the $InVO_4$ and $InVO_4$– TiO_2 was carried out using inductively coupled plasma (ICP-Spectrociros CCD instrument) spectrometer.

The FT-IR spectra of $InVO_4$ and $InVO_4$– TiO_2 were recorded in the 4000– 500 cm^{-1} regionon a Jasco 6300 FT-IR spectrometer with KBr pellets. The diffuse reflectance UV–vis experiments were performed on a Varian Lary 5E diode array spectrometer equipped with a 60-mm Hitachi integrating sphere accessory. The crystal structures of the catalysts ($InVO_4$ and $InVO_4$–TiO_2) were investigated by X-ray diffraction (X-ray diffractometer, Bruker, D8ADVANCE, Germany) with Cu Kα radiation.

Table 1. Structure and characteristics of azo dyes.

Azo dye	Abbreviation	Structure	MW (g mol^{1})	λ_{max} (nm)
Direct Red 23	DR 23	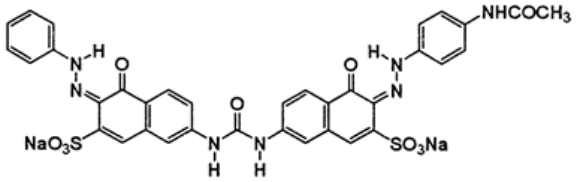	813.72	505
Direct Brown 166	DB 166	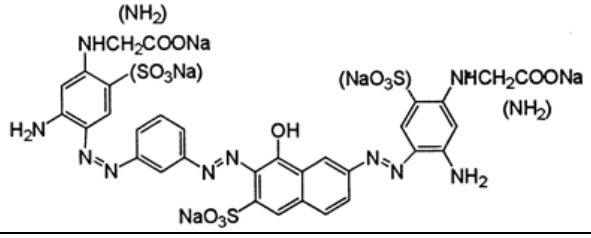	982.73	475

The electron micrographs were obtained using a Cambridge Steroscan S-360 scanning electron microscope (SEM) using an acceleration voltage of 20 Kv and a Philips CM120 transmission electron microscope (TEM). The pH values of the solutions were measured using a digital pH-meter (Metrohm 827). The pH-meter was calibrated with standard buffers at 25°C (pH 4.0 and 7.0). UV–vis spectra of the solutions were recorded with a Jasco 670 UV–vis spectrophotometer with a 1 cm path length cell. The mineralization percent of azo dyes was estimated by total organic carbon (TOC) analyzer. In this regard, TOC curves were obtained with a Beckman 915A analyzer.

2.3. Photocatalytic reactions

The photodegradation of DR 23 and DB 166 was performed in order to evaluate the photocatalytic activity of prepared pure $InVO_4$ and $InVO_4$-TiO_2 nanocomposite. The experiments were carried out in a Pyrex photoreactor with cylindrical shape containing $InVO_4$ or $InVO_4$–TiO_2 (5 mg) and DR 23 or DB 166 solution (10 mL) with an initial concentration of 20 mg/L at different pH (about 3- 10) and at room temperature. The temperature of the suspension was maintained at 25 ± 1 °C by water circulation through an external cooling coil. The optical path length was ca. 2 cm. The light source was a 400 W Na lamp (λ> 450 nm).

The suspension was stirred in the dark for 0-60 min to investigate the dosage of dispersion and adsorption in the absence of light. Due to the dosage of photocatalyst used for degradation of dyes (0.5g/L), no adsorption and/or degradation were observed in the dark. Based on these results, we concluded that the presence of visible light has a significant role in the degradation of dyes.

Moreover, control experiments involving a solution of azo dyes under visible light in the absence of $InVO_4$-TiO_2 nanocomposite were carried out. The results showed that in the absence of $InVO_4$-TiO_2, no degradation was observed. Similar results were obtained in the case of pure $InVO_4$. The lamp was inserted around the suspension after its intensity became stable, photodegradation of dye was carried out in an open vessel in the batch photoreactor. After the reaction was over, the photocatalyst was filtered, and the photolyte was analyzed by UV–vis spectrophotometer at λ_{max} for each dye.

The degradation efficiency (%) was calculated by Eq. 1.

$$\text{Efficiency}\ (\%) = (C_0 - C/C_0) \times 100 \qquad (1)$$

Where C_0 is the initial dyes concentration and C is the concentration of dyes after irradiation.

2.4. Kinetic measurements for degradation of azo dyes

The degradation rate of DR 23 and DB 166 was followed by spectrophotometeric measurements with the time profile of the absorbance being at their λ_{max} (Fig.8). All of the measurements were carried out three times and the mean values of data were reported.

Langmuir–Hinshelwood (L–H) model was used to describe the photocatalytic degradation rate according to Eq. 2 [34].

$$\ln([C]_t/[C]_0) = -k_{obs}t \qquad (2)$$

Where, C_0 is the initial concentration and C_t is the remaining concentration of azo dye at time t. According to the Beer-Lambert law, the absorption (A) of a dissolved substance is a linear function of its concentration. Therefore, the pseudo first order rate constants, k_{obs}, were calculated from the slopes of the natural logarithmic plots of absorption versus time.

2.5. Mineralization

Changes in the TOC values of the suspensions (10 ml of DR 23 or DB 166 solutions with concentrations 20 mg/L in the presence 0.5g/L of $InVO_4$ or $InVO_4$-TiO_2) were determined using a TOC analyzer after filtration at various irradiation time intervals.

3. Results and Discussion

3.1. Characterization of $InVO_4$ and $InVO_4$-TiO_2

The result of elemental analysis [%] for pure $InVO_4$ was calcd: In, 49.98; V, 22.17; Found: In, 47.61; V, 23.35. This result indicated that the measured values are well in consistence with the calculated values, so the rationality of composition of the nanophotocatalyst is confirmed. Moreover, the $InVO_4$ contention the TiO_2 was found to be about 4.3 %.

The FT-IR spectra (Fig. 1) of the $InVO_4$ pure and $InVO_4$-TiO_2 exhibit the absorption characteristic peaks in 1200–450 cm^{-1} region due to $\bar{\nu}$ (V–O), $\bar{\nu}$ (V–O–In) and $\bar{\nu}$ (V–O–V), indicating that $InVO_4$-TiO_2 still retains the basic structure of $InVO_4$ (see Table 2). Furthermore peaks at about 600-500 cm^{-1}, which are related to $\bar{\nu}$ (Ti–O), revealed that $InVO_4$ has been encapsulated.

Table 2. FT-IR data ($\bar{\nu}$/cm^{-1})of the $InVO_4$ and $InVO_4$-TiO_2.

Compound	$\bar{\nu}$ (V-O)	$\bar{\nu}$ (V-O-In)	$\bar{\nu}$ (V-O-V)	$\bar{\nu}$ (Ti-O)
$InVO_4$	1162, 956	903, 718	546, 485	-
$InVO_4$-TiO_2	958, 913	822, 714	546, 503	600-500

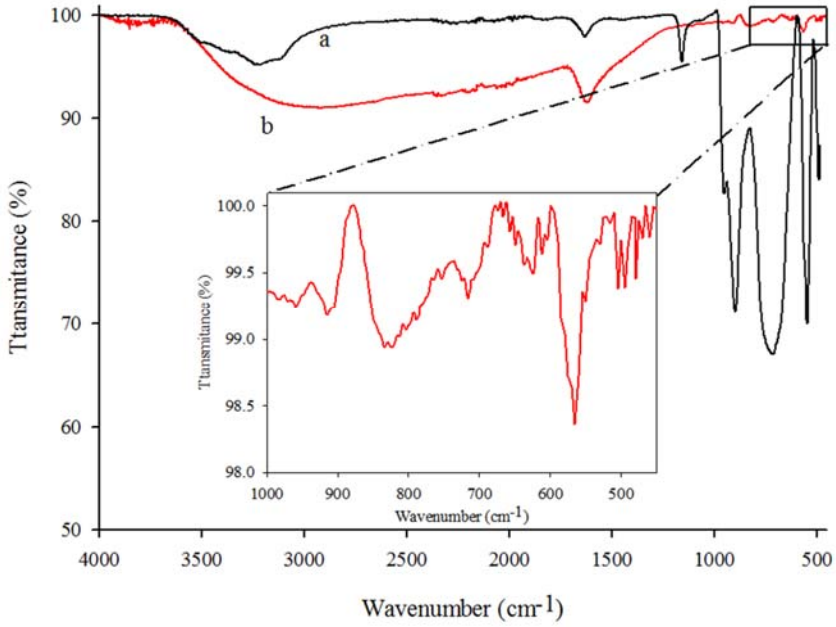

Fig. 1. FT-IR spectra of (a) pure $InVO_4$ and (b) $InVO_4$-TiO_2. Inset shows the enlarged view of the peaks of $InVO_4$-TiO_2 in 1000-450 cm^{-1}.

The absorption bands of about 3200 and 1650 cm^{-1} are assigned to vibrations of hydroxyl group, this is because the samples are not dried enough and have adsorbed some water molecules.

The corresponding DRS for the $InVO_4$-TiO_2 nanocomposite is provided in Fig. 2. Compared with the UV–vis absorption of pure TiO_2 and pure $InVO_4$, the $InVO_4$–TiO_2 nanocomposite exhibits a red-shift. Moreover, the pure $InVO_4$ and $InVO_4$–TiO_2 nanocomposite show absorption peaks in the visible light (~700 nm), while the pure TiO_2 only shows absorption in the UV light region. The difference in absorption edge wavelength for the nanophotocatalysts clearly indicates the band gap of the samples. However, the band gap energy of these photocatalysts was estimated by the following Kubelka-Munk equation (Eq. 3) [35-37].

$$(\alpha h\upsilon) = \beta(h\upsilon - E_g)^n \quad (3)$$

Where, E_g is the semiconductor band gap (eV), h Planck's constant (J s), υ the light frequency (s^{-1}), β the absorption constant, α the absorption coefficient (defined by the Beer–Lambert's law as α = ([2.303 × Abs]/d), where d and Abs are the sample thickness and sample absorbance, respectively.) and n is an index with different values of 1/2, 2, 3/2, and 3 for allowed direct, allowed indirect, forbidden direct and forbidden indirect electronic transitions. The band gap values were calculated using the Tauc method by plotting of $(\alpha h\upsilon)^n$ vs. hυ. Four curves were drawn for the mentioned values for n, and the best linear fitting was obtained for the $(\alpha h\upsilon)^2$ -hυ curve for the $InVO_4$, $InVO_4$-TiO_2 and TiO_2 photocatalysts which agree with the previous literature [38,39]. According to the plot, band gap energies of 3.2, 2.5 and 2.1 eV were estimated for TiO_2, $InVO_4$ and $InVO_4$-TiO_2 photocatalysts, respectively. The band gap of $InVO_4$ is similar to observed values for the 4d (4th row transition metals) compounds such as $InNbO_4$ (2.5 eV) and 5d (5th row transition metals) compounds such as $InTaO_4$ (2.6 eV) [40]. Moreover, the results indicate that visible light absorption of the TiO_2 is enhanced by introducing the $InVO_4$. The $InVO_4$–TiO_2 can be excited by visible light (λ>400 nm, E_g~2.1 eV) and shows the photoactivity under visible light irradiation.

Fig. 3 shows a typical SEM micrographs of pure $InVO_4$ and its nanoencapsulated form ($InVO_4$-TiO_2). Morphological changes represent the encapsulation of $InVO_4$ in TiO_2 nanoparticles. This figure also demonstrates the reduction of $InVO_4$ aggregation due to encapsulation by TiO_2.

The TEM images and the corresponding histograms (Fig. 4) show that pure $InVO_4$ and its nanoencapsulated form ($InVO_4$-TiO_2) uniform and round nanometer particles with a size distribution from 15–55 nm and 4–10 nm, respectively, with the respective maximum in the histogram of particle size distribution at 25–35 and 5–6 nm. From statistical analysis of the particle size, the values of 25.8 nm and 5.7 nm were obtained for the average size of $InVO_4$ and $InVO_4$-TiO_2 nanoparticles, respectively.

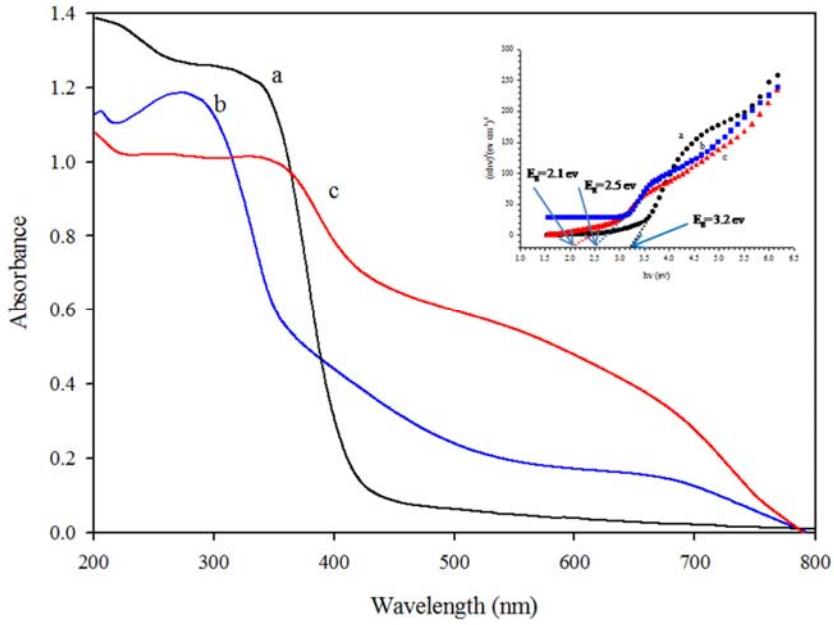

Fig. 2. UV-vis diffusion reflectance spectra of (a) pure TiO_2, (b) pure $InVO_4$ [33] and (c) $InVO_4$–TiO_2 [33]. Inset shows the Tauc plot for band gap energy determination of (a) pure TiO_2, (b) pure $InVO_4$ and (c) $InVO_4$–TiO_2.

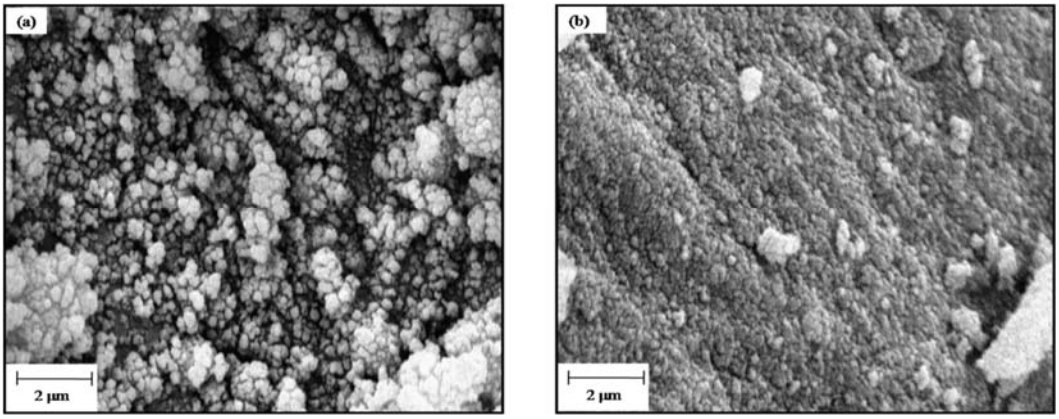

Fig. 3. SEM micrographs of (a) pure $InVO_4$ and (b) $InVO_4$-TiO_2 nanocomposite [33].

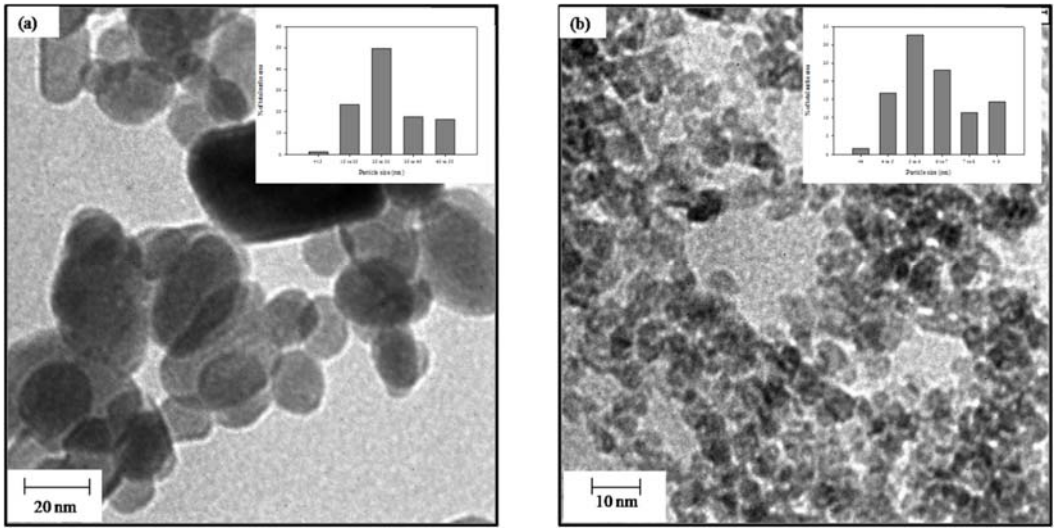

Fig. 4. TEM images and particle size histograms of (a) pure $InVO_4$ and (b) $InVO_4$-TiO_2 nanocomposite.

The XRD technique was used to investigate the phase structures of the samples. The XRD pattern of the as-prepared $InVO_4$, $InVO_4$–TiO_2 and TiO_2 samples are shown in Fig. 5. The XRD peaks in Fig. 5a correspond to the orthorhombic phase of $InVO_4$. The peak at 32.9 was used for calculation of the mean crystallites size. In Fig. 5b, five distinctive TiO_2 peaks are found at 25.3°, 37.9°, 48.0°, 54.6° and 62.8°, which correspond to anatase (101), (103, 004 and 112), (200), (105 and 211), (204) crystal planes, respectively. This XRD pattern is the same as XRD pattern of pure TiO_2 (Fig. 5c), which indicates that the TiO_2 has retained its crystallinity upon mixing with $InVO_4$ and no change in its crystallinity was observed during the preparation of nanocomposite. According to ICP results, the amount of $InVO_4$ is low (<5 %) and it obviously does not present in the XRD pattern of $InVO_4$–TiO_2. The average crystallite sizes were estimated using the XRD line broadening method by Scherrer's equation:

$$d = 0.89\lambda/\beta\cos\theta \quad (4)$$

where, d is the average diameter of the crystal, β is the full width half maximum (FWHM) of the 2θ peak, θ the Bragg angle in degrees and λ the wavelength for CuKα-radiation (λ= 0.1542 nm) [41, 42]. The average crystallite sizes of $InVO_4$ and $InVO_4$- TiO_2 were determined to be 39 nm and 12 nm, respectively.

3.2. Photocatalytic activity

The photocatalytic performance of $InVO_4$-TiO_2 was evaluated by degradation of DR 23 and DB 166 under visible light. The photocatalytic activity of pure $InVO_4$ was also studied under the same conditions for comparison. Photocatalytic degradation of these dyes is influenced by various parameters, such as pH, irradiation time, reaction temperature and dosage of photocatalyst. These reaction parameters were optimized and their optimum values are presented in Table 3.

3.3. pH effect

Fig. 6A displays the visible light activity of $InVO_4$-TiO_2 and pure $InVO_4$ for decomposing DR 23 and DB 166 at different pH values. It was found that the degradation of these dyes by $InVO_4$ and $InVO_4$–TiO_2 are pH dependent and increase by decreasing pH. This can be explained by the PZC of $InVO_4$ and $InVO_4$–TiO_2 nanopowders and a difference in the adsorption ability of $InVO_4$ and $InVO_4$–TiO_2 nanoparticles. For this purpose, The pH_{PZC} of $InVO_4$ and $InVO_4$–TiO_2 nanopowders are determinated by potentiometric mass titrations technique (PMT) according to previous literature [43]. The pH_{pzc} for the $InVO_4$ and $InVO_4$-TiO_2 were estimated about 4.9 and 7.8, respectively (Fig. 6B). Above these pH values, the surface of these catalysts is charged negatively, while below these, it is charged positively. The ionic compounds like DR 23 and DB 166 bearing negative charge can easily be adsorbed on the surface of $InVO_4$ and $InVO_4$–TiO_2 below pH 4.6 and 7.8, respectively. Moreover, the degradation of DR 23 and DB 166 in acidic medium is favorable and due to the electrostatic repulsion, the adsorption ability of $InVO_4$ and $InVO_4$–TiO_2 nanoparticles rapidly decreases in the basic medium.

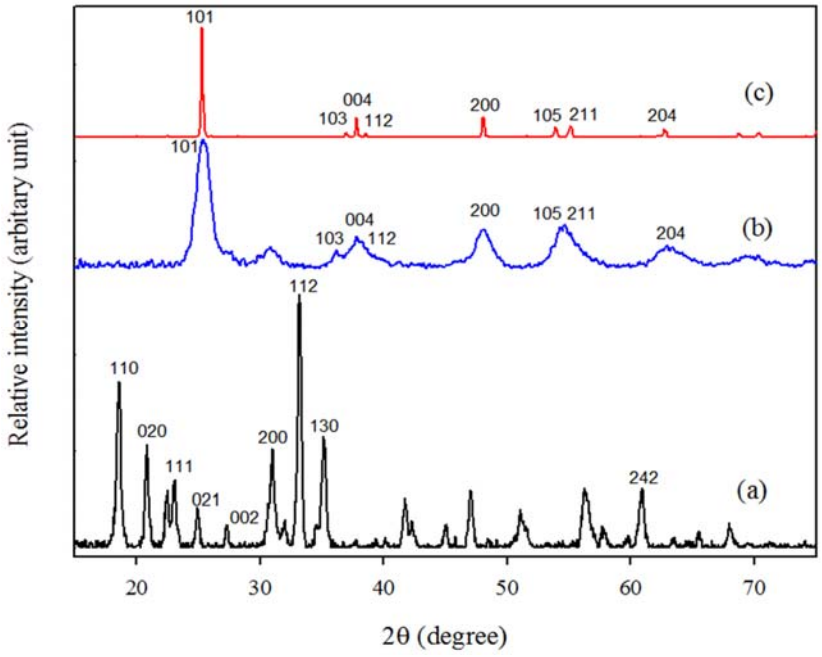

Fig. 5. XRD patterns of (a) pure $InVO_4$, (b) $InVO_4$–TiO_2 and (c) pure TiO_2 [33].

Table 3. The optimum values of different parameters for degradation of DR 23 and DB 166 by $InVO_4$-TiO_2 and pure $InVO_4$ under visible light.

Reaction parameter	$InVO_4$-TiO_2		$InVO_4$	
	Azo dye	Optimum value	Azo dye	Optimum value
pH	DR 23	7.2	DR 23	3.4
	DB 166	7.2	DB 166	3.4
Irradiation time (min)	DR 23	5	DR 23	30
	DB 166	5	DB 166	30
Temperature (°C)	DR 23	25	DR 23	25
	DB 166	25	DB 166	25
Catalyst dosage (g/L)	DR 23	0.5	DR 23	10
	DB 166	0.5	DB 166	10

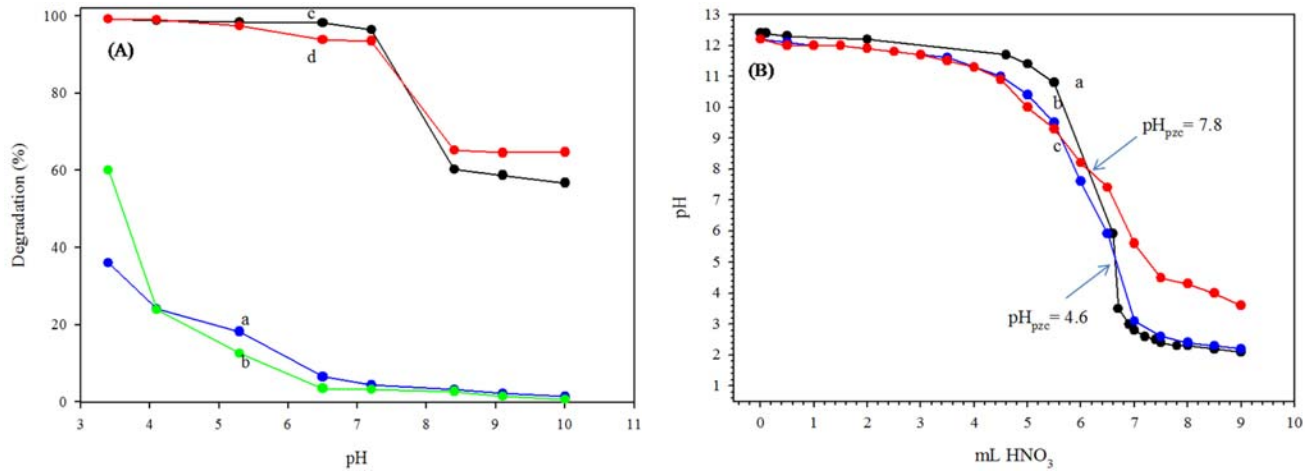

Fig. 6. (A) Effect of pH on degradation percent of (a) DR 23 (20 mg/L) and (b) DB 166 (20 mg/L) in presence pure $InVO_4$ (0.5g/L) and (c) DR 23 (20 mg/L) and (d) DB 166 (20 mg/L) in presence $InVO_4$–TiO_2 (0.5g/L) under visible light for 15 min. (B) Potentiometric mass titrations curves of (a) blank solution (KNO_3, 0.03 M), (b) suspension containing $InVO_4$ (0.5g/L) or (c) $InVO_4$-TiO_2 (0.5g/L) in KNO_3 solution with HNO_3 (0.10 M) for the determination of the pH_{pzc} of $InVO_4$ and $InVO_4$-TiO_2.

However, the maximum dye degradation was observed for pure $InVO_4$ at acidic pH (pH 3.0), while for $InVO_4$-TiO_2, the highest dye degradation was obtained at neutral pH (pH 7.2).

3.4. Time effect

Both the catalyst and a light source are essential for the photocatalysis reaction to occur. A control experiment was carried out on the irradiation of visible light on DR 23 (20 mg/L) and DB 166 (20 mg/L), with and without catalyst, as shown in Fig. 7. There was no degradation noticed in the existence of visible light without any catalysts. In addition about less than 0.2% decrease in dye concentration occurred due to adsorption for the same experiment performed with the catalyst in the absence of visible light. Almost complete degradation was achieved in presence of $InVO_4$–TiO_2 under visible light (60 min) for both azo dyes. In fact, the degradation percent under visible light in the presence of $InVO_4$–TiO_2 nanocomposite increased by increasing the irradiation time and in 5 min, the degradation yields of DR 23 and DB 166 were about 94% and 86%, respectively. The degradation percent reaches a maximum value (20 min) and then, it will be slightly increased. The photocatalytic performance of pure $InVO_4$ which was also evaluated under the same conditions for comparison, is much lower than that of $InVO_4$–TiO_2 at the same time, indicating that the synergistic effect between the two phases can enhance the photocatalytic activity.

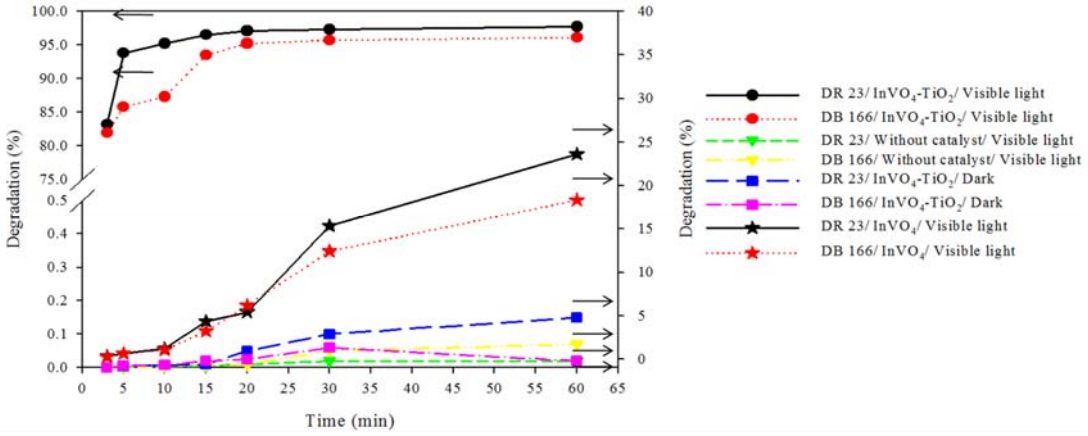

Fig. 7. Effect of time on degradation percent of DR 23 (20 mg/L) and DB 166 (20 mg/L) at pH 7.2.

3.5. Kinetics study

In general, according to a great number of investigations [42,44,45], the dependence of the photocatalytic degradation rates on the concentration of organic pollutants has been described well by the Langmuir–Hinshelwood (L–H) kinetic model. The modified L–H equation is given by:

$$r = -dC/dt = k_r\theta = k_rKC/1 + KC \qquad (5)$$

where k_r is the reaction rate constant, K is the reactant adsorption constant, θ is the fraction of photocatalyst surface coverage and C is the substrate concentration at any time t.

During photocatalytic degradation, intermediates are formed and may interfere in the determination of kinetics because of competitive adsorption and degradation. Therefore, calculations were done at the beginning of irradiation conversion. During a short time interval, any changes such as intermediates effects could be considered as negligible. The photocatalytic degradation rate can be expressed as a function of concentration according to:

$$r_0 = k_rKC_0/1 + KC_0 \qquad (6)$$

where r_0 is the initial rate of photocatalytic degradation of azo dye and C_0 the initial concentration. When the substrate concentration is low enough (less than 20 mg/L in this work) and there is no catalyst saturation, photocatalytic disappearance with $InVO_4$ or $InVO_4$–TiO_2, can follow apparent first-order kinetics. In this case, Eq. (6) can be simplified to a pseudo- first order kinetic model [45].

$$\ln([C]_0/[C]) = k_rKt = k_{app}t \qquad (7)$$

where $k_{app} = k_rK$.

The plot of $\ln([C]_0/[C])$ versus time in Fig. 8 represents straight lines, from which the slope of linear variations equals to the pseudo first order rate constant, k_{app} which was calculated to be 3.82×10^{-1} min^{-1} and 1.36×10^{-1} min^{-1} for DR 23 and DB 166 respectively in presence of $InVO_4$–TiO_2 and 5.00×10^{-3} min^{-1} and 3.00×10^{-3} min^{-1} for DR 23 and DB 166 respectively in presence of pure $InVO_4$.

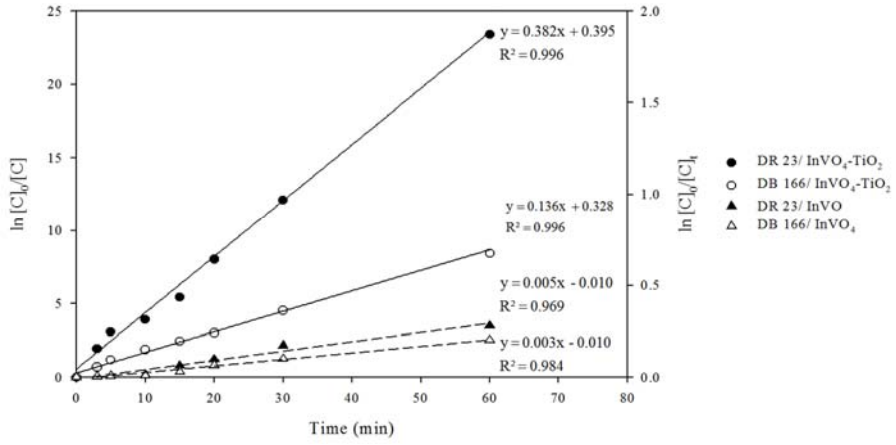

Fig. 8. Kinetic data for photocatalytic degradation of DR 23 (20 mg/L) and DB 166 (20 mg/L) with $InVO_4$-TiO_2 (0.5g/L) and pure $InVO_4$ (0.5g/L).

3.6. Effect of the photocatalyst dosage

The effect of pure $InVO_4$ and $InVO_4$–TiO_2 nanopowder dosage on the photocatalytic degradation of DR 23 (20 mg/L) and DB 166 (20 mg/L) at optimum pH value and using different dosages of nanophotocatalysts (0.3–3.0 g/L) were also studied (Fig. 9). The results showed that the optimum dosage of $InVO_4$–TiO_2 and pure $InVO_4$ catalysts for the degradation of these azo dyes under visible light was 0.5g/L. In general, the total active surface area increased with increasing photocatalyst dosage to a specific level which caused to more photons can be absorbed by the available active sites present in photocatalysts which in turn increased the number of generated hydroxyl and superoxide radicals [34]. As shown, above a specific dosage (0.5g/L in 10 mL azo dye solution (20 mg/L)), the photodegradation activity with a slight slope increases due to aggregation of photocatalyst particles or light scattering [34,46]. Hence, less photocatalyst particles are available for receive photons, so fewer OH radicals are produced.

3.7. Effect of temperature

The results of temperature effect on the photodegradation activity of pure $InVO_4$ or $InVO_4$–TiO_2 (0.5g/L photocatalyst, 20 mg/L DR 23 or DB 166) are shown in Fig. 10. It was observed that with an increase in the temperature from 10 to 80 °C, the percent of degradation with a low average enhancement increased which must be due to the low activation energy of photocatalytic reaction [45,47]. Therefore, the photocatalysis reaction with $InVO_4$ or $InVO_4$–TiO_2 is not very temperature dependent in this case; however, an increase in temperature helps the degradation reaction to compete for more efficiency with electron-hole recombination [45,47]. Higher temperatures cause significant evaporation of the solution during the experiments and also decrease the solubility of oxygen in the water which is not desirable [47]. Thus, a temperature higher than 80 °C is not recommended.

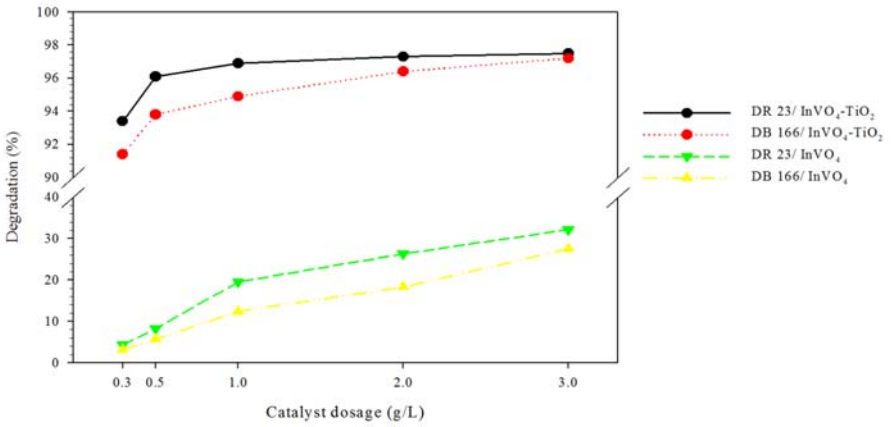

Fig. 9. Effect of Catalyst dosage on degradation percent of DR 23 (20 mg/L) and DB 166 (20 mg/L) at pH 7.2 under visible light for 15 min.

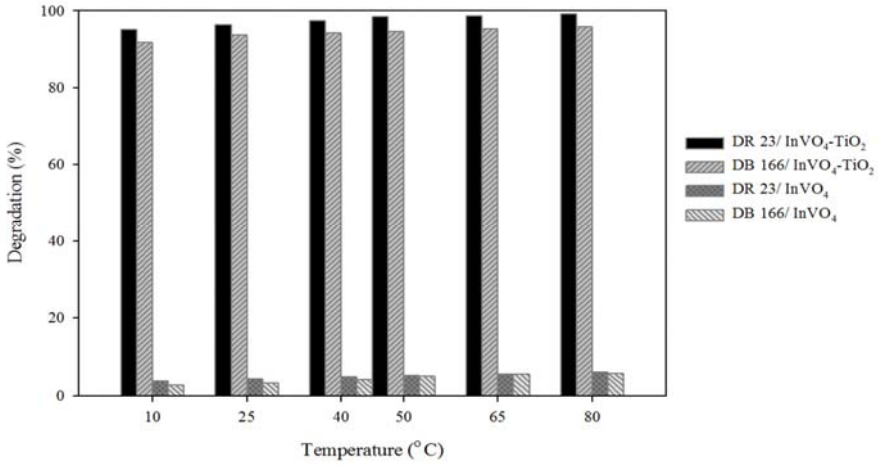

Fig. 10. Effect of temperature reaction on degradation percent of DR 23 (20 mg/L) and DB 166 (20 mg/L) at pH 7.2 with $InVO_4$-TiO_2 (0.5g/L) and pure $InVO_4$ (0.5g/L) under visible light for 15 min.

3.8. Mineralization of DR 23 and DB 166

Changes in the TOC values reflect the degree of degradation or mineralization of an organic substrate during the irradiation period. Fig.11 shows the changes in TOC and mineralization percent during the degradation of DR 23 and DB 166 solutions in the presence of $InVO_4$ and $InVO_4$-TiO_2. It was observed that the total mineralization increases by increasing the irradiation time and happens after complete decolorization of these azo dyes. Interestingly, the change in TOC values is very similar to the degradation kinetics: The $InVO_4$-TiO_2 is more efficient in degrading these azo dyes compared to pure $InVO_4$.

3.9. Photocatalytic Mechanism of $InVO_4$-TiO_2

On the basis of the aforementioned results, the potential electrons transfer route and photocatalytic mechanism for DR 23 and DB 166 degradation over $InVO_4$-TiO_2 hetero-structure is shown in Scheme 1. Under visible light irradiation, $InVO_4$ can be excited to produce h^+ and e^-. Under normal conditions, most of the electrons–holes pairs recombine rapidly, thus pure $InVO_4$ has a respectively low photocatalytic activity. Due to the well-matched overlapping band-structures and intimate interfaces of TiO_2/$InVO_4$, photogenerated electrons on the CB of $InVO_4$ can migrate to the CB of TiO_2 (electron transfer I: $InVO_4$ (CB)→TiO_2 (CB)) and then react with adsorbed O_2 to produce superoxide radical ($O_2^{-}\cdot$), which enhance the separation efficiency of photogenerated electrons and holes of $InVO_4$. The $O_2^{-}\cdot$can react with H^+ to produce hydroxyl radical ($OH\cdot$). Both these radicals are strong oxidants that can completely oxidize organic molecules to mineral acids, H_2O and CO_2 [48].

4. Conclusions

Effective photodegradation of the two non-biodegradable azo dyes (DR 23 and DB 166) is available using pure $InVO_4$ or $InVO_4$–TiO_2 nanocomposite suspended aqueous solutions and during short times of visible irradiation when compared with only photodegradation process. There is an optimum dosage of suspended $InVO_4$ or $InVO_4$–TiO_2 photocatalyst at which the highest degradation efficiency for 20 mg/L of DR 23 or DB 166 will be available. However, this degradation is not significantly affected by temperature. With the aim of the highest degradation, the best conditions using pure $InVO_4$ are photocatalyst dosage= 0.5 g/L, pH= 3.0 and ambient temperature= 25 °C and in the presence of $InVO_4$–TiO_2, the moderate conditions for the highest degradation are: photocatalyst dosage= 0.5 g/L, pH= 7.2 (natural pH) and ambient temperature= 25 °C. Under these conditions, for degradation efficiency of more than 20% and 90% of substrates, 60 min and 15 min (using $InVO_4$ and $InVO_4$–TiO_2, respectively) visible irradiation time is required. The results clearly indicate that coupling of two photocatalysts has an important role to enhance their photocatalytic activity. It is due to the alignments of the electronic band structures of TiO_2 and $InVO_4$, the photogenerated electrons in the CB of $InVO_4$ can be quickly transferred to the CB of TiO_2. The photogenerated charge separation at the interfaces of $InVO_4$-TiO_2 suppresses the recombination of photogenerated electron-hole pairs and leads to an enhanced photocatalytic performance of $InVO_4$-TiO_2. The photocatalytic degradation shows pseudo first order kinetics.

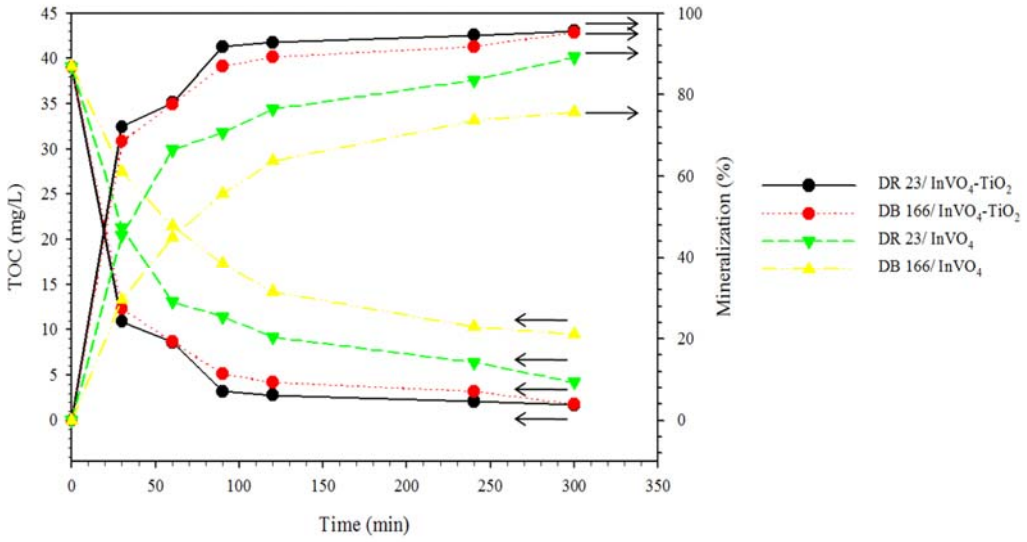

Fig. 11. Changes of TOC and mineralization percent during degradation of DR 23 (20 mg/L) and DB 166 (20 mg/L) at optimum pH under visible light in the presence of pure $InVO_4$ (0.5g/L) and $InVO_4$-TiO_2 (0.5g/L).

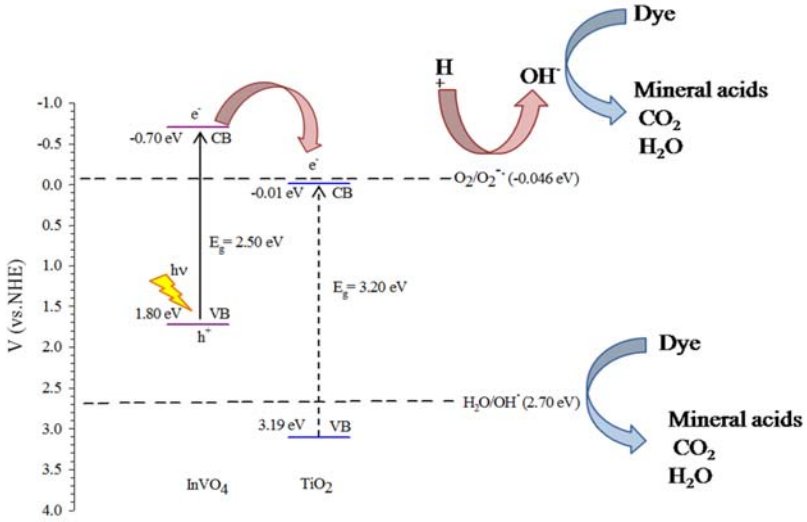

Scheme 1. Schematic illustration of the charge separation and photocatalytic mechanism of $InVO_4$- TiO_2 heterostructure under visible light irradiation.

The rate constant of photodegradation process of these azo dyes in the presence of $InVO_4$–TiO_2 is more (about 100 times) with respect to the case of pure $InVO_4$. The TOC analysis revealed that complete mineralization of dyes can be achieved in longer irradiation times (300 min) than dye decolorization.

Acknowledgements

The authors gratefully acknowledge the financial support of this work by the Research Council of University of Hormozgan and Iran National Science Foundation (INSF-941219).

References

[1] V. Eskizeybek, F. Sarı, H. Gülce, A. Gülce, A. Avcı, Appl. Catal. B 119–120 (2012) 197-206.
[2] H.R. Pouretedal, M. Ahmadi, Iran. J. Catal. 3 (2013) 149-155.
[3] L. Vafayi, S. Gharibe, Iran. J. Catal. 5 (2015) 365-371.
[4] A. Buthiyappan, A.R. Abdul Aziz, W.M. Ashri Wan Daud, Rev. Chem. Eng. 32 (2016) 1-47.
[5] M. Karimi-Shamsabadi, A. Nezamzadeh-Ejhieh, J. Mol. Catal. A: Chem. 418 (2016) 103-114.
[6] E.P. Chagas, L.R. Durrant, Enzyme Microb. Technol. 29 (2001) 473-477.
[7] M. Stylidi, D.I. Kondarides, X.E. Verykios, Appl. Catal. B 40 (2003) 271-286.
[8] I.K. Konstantinou, T.A. Albanis, Appl. Catal. B 49 (2004) 1-14.
[9] C. Feng, X. Zhuo, X. Liu, J. Rare Earth 27 (2009) 717-722.
[10] M.A. Fox, M.T. Dulay, Chem. Rev. 93 (1993) 341-357.
[11] M.A. Rauf, M.A. Meetani, S. Hisaindee, Desalination 276 (2011) 13-27.
[12] B. Khodadadi, Iran. J. Catal. 6 (2016) 305-311.
[13] A. Nezamzadeh-Ejhieh, Z. Ghanbari-Mobarakeh, J. Ind. Eng. Chem. 21 (2015) 668-676.
[14] R. Asahi, T. Morikawa, T. Ohwaki, K. Aoki, Y. Taga, Science 293 (2001) 269-271.
[15] M. Grätzel, Nature 414 (2001) 338-344.
[16] S.U. Khan, M. Al-Shahry, W.B. Ingler, Science 297 (2002) 2243-2245.
[17] K. Maeda, T. Takata, M. Hara, N. Saito, Y. Inoue, H. Kobayashi, K. Domen, J. Am. Chem. Soc. 127 (2005) 8286-8287.
[18] W. Zhao, W. Ma, C. Chen, J. Zhao, Z. Shuai, J. Am. Chem. Soc. 126 (2004) 4782-4783.
[19] Z. Zou, J. Ye, K. Sayama, H. Arakawa, Nature 414 (2001) 625-627.
[20] A. Rostami-Vartooni, M. Nasrollahzadeh, M. Salavati-Niasari, M. Atarod, J. Alloys Compd. 689 (2016) 15-20.
[21] H. Fallah Moafi, Iran. J. Catal. 6 (2016) 281-292.
[22] J. Yang, Y. Kim, Y. Shul, C. Shin, T. Lee, Appl. Surf. Sci. 121 (1997) 525-529.
[23] A. Sclafani, L. Palmisano, G. Marcı, A. Venezia, Sol. Energy Mater. Sol. Cells 51 (1998) 203-219.
[24] L. Zang, W. Macyk, C. Lange, W.F. Maier, C. Antonius, D. Meissner, H. Kisch, Chem. Eur. J. 6 (2000) 379-384.
[25] D. Dvoranova, V. Brezova, M. Mazúr, M.A. Malati, Appl. Catal. B 37 (2002) 91-105.
[26] N. Ajoudanian, A. Nezamzadeh-Ejhieh, Mater. Sci. Semicond. Process 36 (2015) 162-169.
[27] H. Derikvandi, A. Nezamzadeh-Ejhieh, J. Colloid Interface Sci. 490 (2017) 652-464.
[28] U. Bach, D. Lupo, P. Comte, J. Moser, F. Weissörtel, J. Salbeck, H. Spreitzer, M. Grätzel, Nature 395 (1998) 583-585.
[29] J.C. Yu, L. Wu, J. Lin, P. Li, Q. Li, Chem. Commun. (2003) 1552-1553.
[30] M. Oshikiria, M. Boero, J. Ye, Z. Zou, G. Kido, J. Chem. Phys. 117 (2002) 7313-7318.
[31] M. Oshikiri, M. Boero, J. Ye, F. Aryasetiawan, G. Kido, Thin Solid Films 445 (2003) 168-174.

[32] J. Tang, Z. Zou, J. Ye, Chem. Mater. 16 (2004) 1644-1649.
[33] S. Dianat, S. Tangestaninejad, V. Mirkhani, M. Moghadam, I. Mohammadpoor-Baltork, J. Iran. Chem. Soc. 10 (2013) 535-544.
[34] J. Esmaili-Hafshejani, A. Nezamzadeh-Ejhieh, J. Hazard. Mater. 316 (2016) 194-203.
[35] M. Babaahamdi-Milani, A. Nezamzadeh-Ejhieh, J. Hazard. Mater. 318 (2016) 291-301.
[36] A. Shirzadi, A. Nezamzadeh-Ejhieh, J. Mol. Catal. A: Chem. 411 (2016) 222-229.
[37] S. Jafari, A. Nezamzadeh-Ejhieh, J. Colloid Interface Sci. 490 (2017) 478-487.
[38] J. Ye, Z. Zou, M. Oshikiri, A. Matsushita, M. Shimoda, M. Imai, T. Shishido, Chem. Phys. Lett. 356 (2002) 221-226.
[39] C.S. Enache, D. Lloyd, M.R. Damen, J. Schoonman, R. van de Krol, J. Phys. Chem. C 113 (2009) 19351-19360.
[40] Z. Zou, J. Ye, H. Arakawa, Chem. Phys. Lett. 332 (2000) 271-277.
[41] M. Bordbara, S. Forghani-Pileroodb, A. Yeganeh-Faalb, Iran. J. Catal. 6 (2016) 415-421.
[42] A. Nezamzadeh-Ejhieh, S. Hushmandrad, Appl. Catal. A 388 (2010) 149-159.
[43] J. Vakros, C. Kordulis, A. Lycourghiotis, Chem. Commun. (2002) 1980-1981.
[44] A. Nezamzadeh-Ejhieh, M. Khorsandi, Iran. J. Catal. 1 (2011) 99-104.
[45] J. Saien, S. Khezrianjoo, J. Hazard. Mater. 157 (2008) 269-276.
[46] A. Besharati-Seidani, Iran. J. Catal. 6 (2016) 447-454.
[47] Z. Shams-Ghahfarokhi, A. Nezamzadeh-Ejhieh, Mater. Sci. Semicond. Process. 39 (2015) 265-275.
[48] X. Lin, D. Xu, Z. Lin, S. Jiang, L. Chang, RSC Adv. 5 (2015) 84372-84380.